

Article

Contactless Blood Pressure Estimation System Using a Computer Vision System

Ali Al-Naji ^{1,2,*} , Ahmed Bashar Fakhri ¹ , Mustafa F. Mahmood ¹ and Javaan Chahl ^{2,*} ¹ Electrical Engineering Technical College, Middle Technical University, Baghdad 10022, Iraq² School of Engineering, University of South Australia, Mawson Lakes, SA 5095, Australia

* Correspondence: ali_al_naji@mtu.edu.iq (A.A.-N.); javaan.chahl@unisa.edu.au (J.C.);

Tel.: +964-771-030-4768 (A.A.-N.)

Abstract: Blood pressure (BP) is one of the most common vital signs related to cardiovascular diseases. BP is traditionally measured by mercury, aneroid, or digital sphygmomanometers; however, these approaches are restrictive, inconvenient, and need a pressure cuff to be attached directly to the patient. Therefore, it is clinically important to develop an innovative system that can accurately measure BP without the need for any direct physical contact with the people. This work aims to create a new computer vision system that remotely measures BP using a digital camera without a pressure cuff. The proposed BP system extracts the optical properties of photoplethysmographic signals in two regions in the forehead captured by a digital camera and calculates BP based on specific formulas. The experiments were performed on 25 human participants with different skin tones and repeated at different times under ambient light conditions. Compared to the systolic/diastolic BP readings obtained from a commercial digital sphygmomanometer, the proposed BP system achieves an accuracy of 94.6% with a root mean square error (RMSE) of 9.2 mmHg for systolic BP readings and an accuracy of 95.4% with an RMSE of 7.6 mmHg for diastolic BP readings. Thus, the proposed BP system has the potential of being a promising tool in the upcoming generation of BP monitoring systems.

Keywords: contactless BP monitoring; face detection; video plethysmography; digital camera



Citation: Al-Naji, A.; Fakhri, A.B.; Mahmood, M.F.; Chahl, J. Contactless Blood Pressure Estimation System Using a Computer Vision System. *Inventions* **2022**, *7*, 84. <https://doi.org/10.3390/inventions7030084>

Academic Editors: Edwin Lughofer and Byungun Yoon

Received: 26 July 2022

Accepted: 15 September 2022

Published: 18 September 2022

Publisher's Note: MDPI stays neutral with regard to jurisdictional claims in published maps and institutional affiliations.



Copyright: © 2022 by the authors. Licensee MDPI, Basel, Switzerland. This article is an open access article distributed under the terms and conditions of the Creative Commons Attribution (CC BY) license (<https://creativecommons.org/licenses/by/4.0/>).

1. Introduction

Monitoring of blood pressure (BP) is considered one of the essential indicators of human health that helps to detect and manage cardiovascular diseases. According to the World Health Organization (WHO) [1], cardiovascular diseases are the leading cause of 32% of all global deaths, and about 17.9 million people globally died in 2019 from cardiovascular diseases. Furthermore, in the last three decades, the number of adults diagnosed with hypertension has risen from 650 million to 1.28 billion worldwide [2]. Current instrumentations for measuring BP are based on mechanical or oscillometric recordings, such as a mercury sphygmomanometer, an aneroid sphygmomanometer, or a digital sphygmomanometer. These instrumentations, however, are cuff-based measurement methods that are directly attached to the patient's upper arm or wrist, which can be uncomfortable and cumbersome for repeated measurements or for long-term monitoring. Moreover, the BP readings are easily affected by unskilled examiners and cannot achieve continuous BP monitoring [3]. In addition, physical access to patients during the COVID-19 pandemic is another challenge for these contact instruments [4]. Therefore, a significant need exists for innovative systems that can accurately measure BP and assess cardiovascular risk when physical contact with the patients is either undesirable or unsafe.

In recent years, a computer vision system based on plethysmographic signals (extracting color variations at the skin's surface that contains a wealth of physiological information using a camera as a photodetector) has attracted considerable attention as a technique to

measure BP. Previous attempts have tested contact finger-based video plethysmography using smartphones along with the corresponding electrocardiogram (ECG) signal to measure pulse transit time (PTT) and to estimate the related BP [5–10]. Despite the contact finger-based video plethysmography offering some advantages, it may expose patients to the risk of infection and skin irritation as well as being unsuitable for people with skin ulcers, burns, congenital and contagious conditions [11–14]. To address the limitations mentioned above while reducing the wiring and increasing safety, the development of contactless BP monitoring systems is increasingly desirable.

Recent studies have proved that video plethysmography could be used to remotely measure cardiac activity, including BP. For example, McDuff et al. [15] proposed a new imaging system based on a digital camera to remotely measure the cardiovascular blood volume pulse (BVP) detected via plethysmographic signals from the face using ambient light at a distance of 3 m. Then, they used an independent component analysis (ICA) technique followed by a bandpass filter (0.75–4.5 Hz) to extract the signal of interest and applied a peak detection method to detect the systolic and diastolic peaks, where the head motion and light conditions were the main challenges in their study. Another example, a study by Murakami et al. [16] measured PTT signals from two regions (wrist and ankle) using a digital camera. The study used a finite impulse response (FIR) low pass filter (2 Hz) as noise removal, phase delay compensation, and a peak detection method to extract pulse peaks at both regions and investigated their relationship to systolic blood pressure. However, the regions of interest (ROI) should be clear, and the subject should lie down on a bed during the measurement, and removal of garments may be required. Another study by Secerbegovic et al. [17] used a digital camera as a plethysmographic detector in combination with an electrocardiogram (ECG) to measure PTT signals from two regions (forehead and palm) and predict only systolic blood pressure using the ICA technique. The selected signal was then filtered with a band of 0.6 to 4 Hz. However, synchronizing plethysmographic signals with ECG signals was required due to the reflection of the pressure waves, sensor noise, and some movement considerations. Patil et al. [18] proposed a non-contact imaging system for BP measurement using plethysmographic signals from the forehead captured by a webcam. Their study also used ICA on the plethysmographic signal, and then leveraging features extracted from the output signals as inputs to a neural network system. However, their study was affected by lighting conditions and noise because the PTT is affected by variations in distance between the camera sensor and the selected ROIs. Another work by Sugita et al. [19] presented a new imaging system to predict BP variability using a pulse wave obtained from video plethysmography at three regions (right palm, forehead, and right cheek) without calculating the PTT. The plethysmographic signals were then directly filtered (around 1 Hz) to extract the heartbeat-related component. This study, however, was tested using an external LED light source, and there were individual differences in the correlation of the proposed system with BP. Fan et al. [20] proposed a developed contactless imaging system to estimate BP after improving and detecting the peaks in the PTT signal obtained from video plethysmography from two regions (face and palm). The study improved the PTT using an adaptive Gaussian fitting model because the relationship between BP and PTT is not completely linear. A remote estimation of pulse wave features related to BP and arterial stiffness based on a computer vision system was proposed by Djeldjli et al. [11]. A digital camera and contact probes (finger and earlobe sensors) in association with an external light source were utilized to capture the video plethysmography and contact plethysmographic signals. The extracted signals were then filtered using a finite impulse response high-pass filter and continuous wavelet transform with a bandwidth of 0.5–4 Hz. A Contactless BP measurement based on video plethysmography and PTT was also proposed by [21]. The proposed system was then improved by using a neural network for training and BP prediction. A recent study by Iuchi et al. [22] used a digital camera to estimate continuous BP by continually tracking spatial information of facial pulse waves based on a convolutional neural network (CNN). However, the accuracy of the neural network systems remains dependent on the

accuracy of the training data. Due to the natural characteristics of the plethysmographic signal, some physiological information often disappears for two reasons. The first reason is the surrounding environment, camera sensor, and light-transmitting properties of the skin, and the second reason is the loss of physiological information due to component analysis, signal filtering, and peak detection, requiring a number of challenges to be considered. As reported in Cheng et al. [23], the plethysmographic signals could be recovered from the effect of lighting changes by decomposing the green channel of the facial ROI into a set of signals with different scales of time series using an ensemble empirical mode decomposition of the Hilbert–Huang transform instead of ICA that works with motion artifacts. Therefore, this study proposes a contactless imaging system based on video plethysmography that overcomes the limitations mentioned above using an effective method that is tolerant of lighting changes during measurement. The proposed BP system used an adaptive decomposition method called a complete ensemble empirical mode to decompose the plethysmographic signals captured in two regions on the forehead into a set of signals with different scales of time series, and selecting the signals with the best frequency spectra that correspond to cardiac activity to achieve a remote estimate of BP without using component analysis, filtering and peak detection that will operate under ambient illumination conditions.

The remainder of this paper consists of the following: Section 2 describes the materials and methods of the study, including research ethics and participants, experimental setup, and system overview. Section 3 presents the results and statistical analysis of the proposed imaging system performed on human participants with discussion. Finally, Section 4 concludes the paper.

2. Materials and Methods

2.1. Research Ethics and Participants

The study followed the principles outlined in the Declaration of Helsinki and received ethical approval from the research committee in the Training and Human Development Centre, Ministry of Health and Environment, Iraq (research protocol number: 1040). The participant information sheet and written consent forms were collected electronically with the possibility of withdrawing before the completion of data collection. Before starting the experiment, all participants were informed about how they will save and protect their personal data after completing the study. A total of 25 participants (18 males and 7 females) without any known cardiovascular disease aged from 18 to 60 years with different skin tones took part in the research study.

2.2. Experimental Setup

The experimental setup includes a digital camera (Nikon D5300, 10 MP, 18–55 mm Lens) mounted on a tripod and a commercial blood pressure monitor (Rossmax, Harrisburg, PA, USA) as a benchmark device. Prior to the measurements, all participants were asked to rest on a chair for several minutes to ensure a stable physiological state and then asked to face the camera at a distance of approximately 50 cm, as shown in Figure 1. They were also asked not to move and to breathe gently during video capture. Four video recordings from each participant were performed at different times. A total of 100 video data (10 s length) were collected with a resolution of 1920×1080 pixels at a frame rate of 60 frames per second and saved in MOV format without any compression. The experiments were conducted under ambient illumination conditions without any additional light sources.

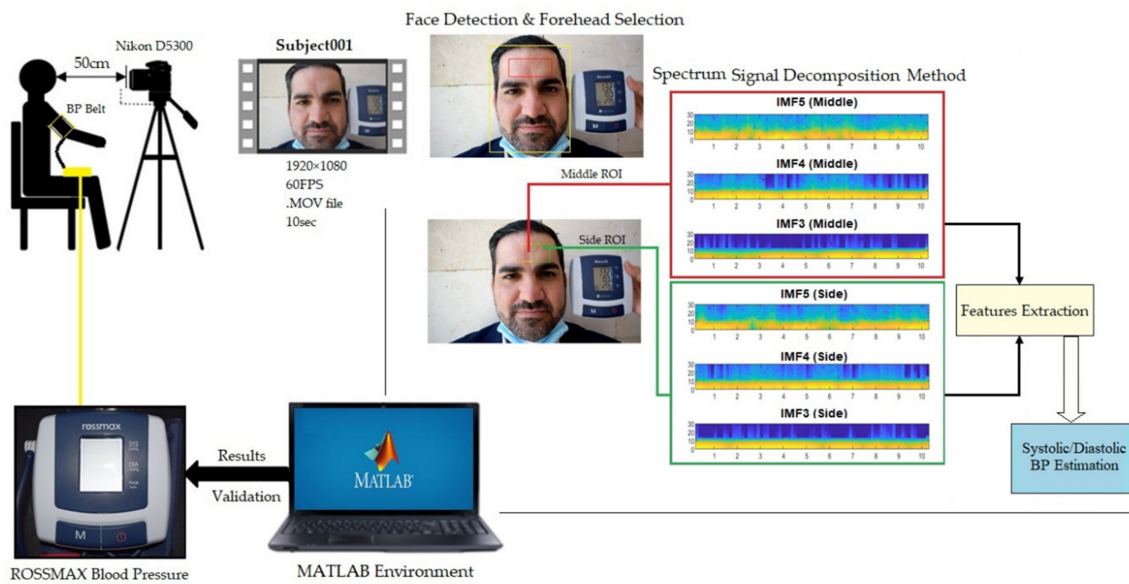


Figure 1. Demonstrating the proposed imaging system that recorded videos by a digital camera and processed the obtained signals while simultaneously recording the BP readings from a contact pressure cuff device for validation purposes.

2.3. System Overview

The framework of the proposed imaging system was designed to extract the cardiac relevant plethysmographic signals from the selected forehead regions and decompose the extracted plethysmographic signals into a set of signals with different scales of time series, as demonstrated in Figure 1.

The block diagram of the proposed imaging system is shown in Figure 2. As can be seen, the proposed imaging system consists of several main parts, including face and forehead detection, ROIs selection, signal decomposition, features extraction, and a determination of blood pressure ratio.

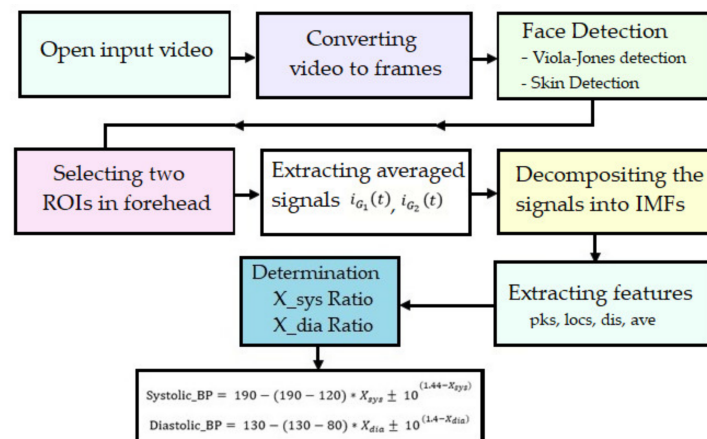


Figure 2. The block diagram of the proposed imaging system.

The process is conducted by firstly converting the videos into frames. Then, the Viola-Jones detection method [24] is used to detect the facial region automatically. Kanade Lucas-Tomasi (KLT) feature extraction is used to detect the face in the first frame and then the extracted features across the video frames were used to continue tracking the facial region. This method is used due to its accuracy and low computational cost [25,26]. To increase the robustness of the proposed imaging system, a skin detection method based on multi-level thresholding is used as an alternative for face detection if the Viola-Jones

detection method fails to detect the face due to background clutter issues. Multi-level thresholding is an image segmentation method that applies two or more threshold values in YCbCr color space. The forehead region is chosen as ROI because it is least affected by facial expressions, talking, and eye blinking. The selected ROI is then divided into two regions: the middle region (ROI₁) and the side region (ROI₂), as shown in Figure 3.

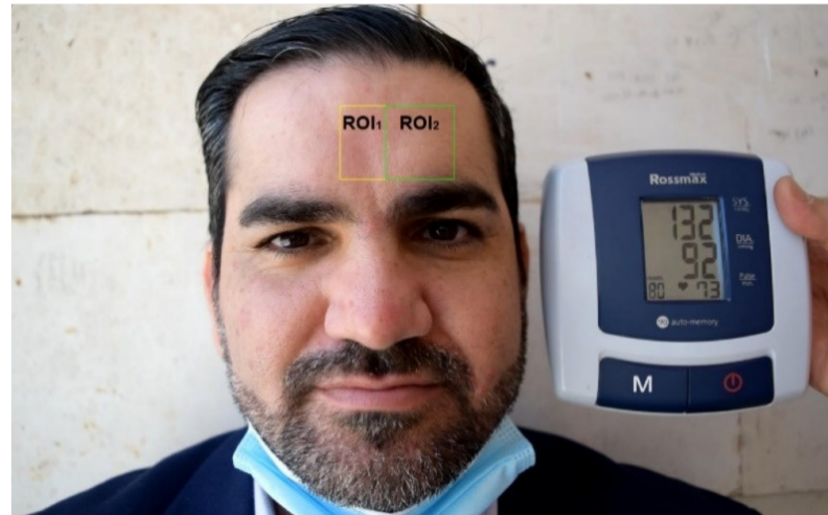


Figure 3. The selected forehead regions: the middle region (ROI₁) and the side region (ROI₂).

Green channel (G) was selected from RGB color space since this component reportedly contains the strongest plethysmographic signals [27–29]. The required G values in the ROIs are processed for the computation of the photoplethysmograph. The time-series plethysmographic signals from ROI₁ and ROI₂ were extracted by averaging the pixels values for each frame in the selected video as follows: [30]

$$i_{G_1}(t) = \frac{\sum_x^{H_1} \sum_y^{W_1} F_i(x, y)}{H_1 \times W_1} \quad (1)$$

$$i_{G_2}(t) = \frac{\sum_x^{H_2} \sum_y^{W_2} F_i(x, y)}{H_2 \times W_2} \quad (2)$$

where H_1 is the height of the selected middle forehead region ROI₁ in pixels, W_1 is the width of the ROI₁ in pixels, H_2 is the height of the selected side forehead region ROI₂ in pixels, W_2 is the width of the ROI₂ in pixels, and $F_i(x, y)$ represents the light level of the G component plane at the (x, y) coordinates of frame i , where the averaged values for Equations (1) and (2) are in a range from 0–255.

Since the averaged pixel values can be affected by illumination variation noise, a complete ensemble empirical mode decomposition method [31] is used to separate the cardiac pulse signal in plethysmographic signals from the illumination variation noise without the need to filter the signal. This decomposition method is commonly used to remove illumination noise artifacts from plethysmographic signals [23,32,33]. This method is a noise-assisted adaptive data analysis method developed by Colominas et al. [31] to improve the decomposition of nonstationary and nonlinear signals into several signals with different scales of time series, called intrinsic mode functions (IMFs). It decomposes signals based on local characteristics of signals by adding positive and negative white noises to signals, thus avoiding the undesired mode mixing problem and achieving a negligible reconstruction error, presented in previous mode decomposition methods [34–36]. This method adds a noise-adding scheme at each stage of the decomposition and calculates a unique residue to obtain each IMF, making the obtained signals almost complete. In addition, selecting the optimal maximum number of sifting iterations can reduce execution

time for this decomposition method. By applying this decomposition method, $i_G(t)$ from each region is composed into a finite number of IMFs, as shown in Figure 4.

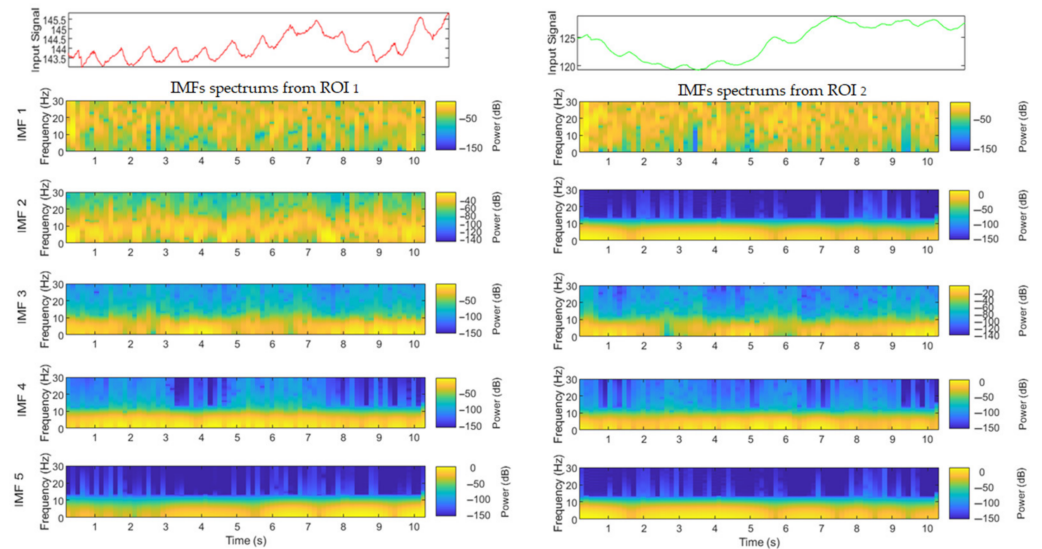


Figure 4. Signal decomposition of $i_{G1}(t)$ and $i_{G2}(t)$ using a decomposition method with 100 realizations and 100 iterations.

As illustrated in Figure 4, each signal is decomposed into five signals with different frequencies. IMFs signals were analyzed in the time-frequency domains using MATLAB built-in command, called “pspectrum”. This command uses spectrogram function to returns a vector of time-series signal corresponding to the centers of the windowed segments used to estimate power spectrum of the selected signal. This function helps to visualize interference features embedded within the selected signal at a time resolution of 0.5 s and zero overlap between adjoining segments. Three IMFs (IMF3, IMF4 and IMF5) from each region with the largest maximal amplitude are selected as candidates to estimate BP and neglecting IMF1 and IMF2 that fall within the possible light changes frequencies to reduce the illumination noise artifacts, as shown in Figure 5.

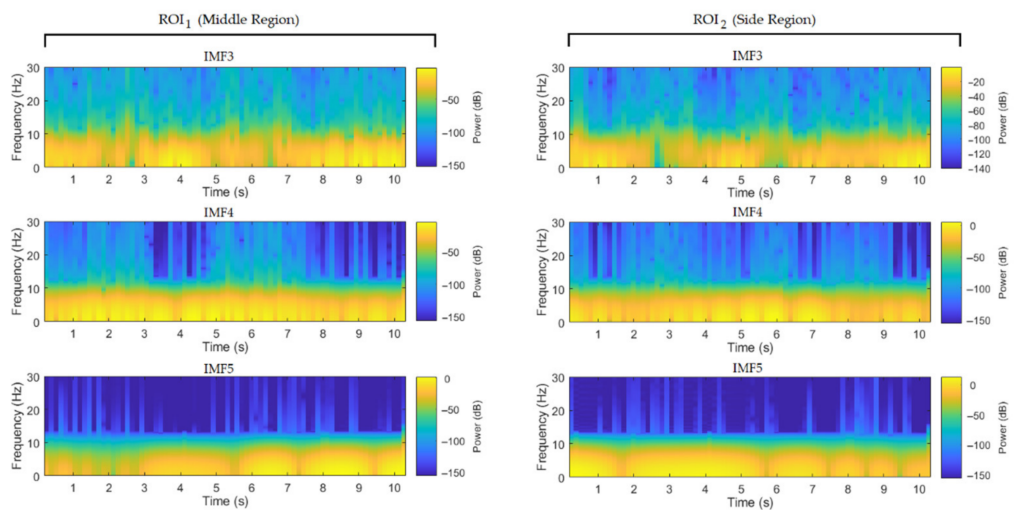


Figure 5. The selected IMF spectrums from ROI₁ and ROI₂ at a time resolution of 0.5 s.

Then, the features (locations of peaks and the distance between the consecutive peaks) from the selected IMFs are extracted to estimate BP. The following formula is used to estimate the ratio of systolic BP as follows:

$$X_{sys} = \frac{dx_1 + dy_1}{dz_1} \tag{3}$$

where x is the distance between the first two consecutive peaks from IMF4 (ROI₁), y is the distance between the first two consecutive peaks from IMF5 (ROI₁), z is the average distance among the peaks from IMF3 (ROI₂), $dx_1 = x^{0.33}$, $dy_1 = y^{0.25}$ and $dz_1 = 2(1 + z)$. The systolic BP can then be calculated using the following formula

$$\text{Systolic BP} = (190 - [(190 - 120) \times X_{sys}] \pm dt_1 \tag{4}$$

where $d_{t1} = 10^{(1.44 - X_{sys})}$ where 1.44 is a value of X_{sys} corresponding to systolic BP that equals approximately 90 mmHg.

- If ($X_{sys} > 1$), the value of d_{t1} will be added to Equation (4)
- If ($X_{sys} < 1$), the value of d_{t1} will be subtracted from Equation (4)
- If ($X_{sys} = 1$), the value of d_{t1} will be ignored.

The following formula is used to estimate the ratio of diastolic BP as follows:

$$X_{dias} = \left[\frac{dx_2 + dy_2 + \frac{1}{dx_2}}{2} \right] - dz_2 \tag{5}$$

where $dx_2 = x^{0.25}$, $dy_2 = y^{0.33}$, and $dz_2 = 2z$

$$\text{Diastolic BP} = (130 - [(130 - 80) \times X_{dias}] \pm dt_2 \tag{6}$$

where $d_{t2} = 10^{(1.4 - X_{dias})}$ where 1.4 is a value of X_{dias} corresponding to diastolic BP that equals approximately to 60 mmHg.

- If ($X_{dias} > 1$), the value of d_{t2} will be added to Equation (6)
- If ($X_{dias} < 1$), the value of d_{t2} will be subtracted from Equation (6)
- If ($X_{dias} = 1$), the value of d_{t2} will be ignored.

3. Experimental Results and Discussion

The videos and extracted signals were processed offline using the MATLAB program (MathWork Inc., Natick, MA, USA). For system verification, the results of the proposed imaging system were evaluated against their corresponding benchmark (BM) measurements using statistical parameters, such as accuracy, root mean square error (RMSE), mean absolute error (MAE), absolute percentage error (APE), mean absolute percentage error (MAPE). The comparison between systolic/diastolic BP readings against their BM readings for all collected data is shown in Figure 6.

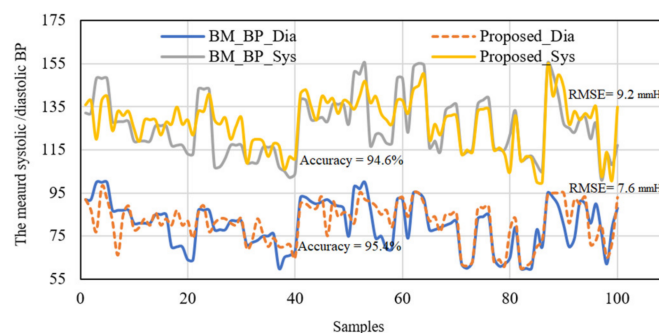


Figure 6. The systolic and diastolic BP comparison between the proposed imaging system and BM measurements.

It is clear from Figure 6 that the accuracy of the proposed imaging system for systolic BP measurements was 94.6% with an RMSE of 9.2 mmHg, while it was 95.4% for diastolic BP measurements with an RMSE of 7.6 mmHg. The error ratios, including MAE and MAPE of the measured systolic BP readings, were also examined with respect to those of the BM measurements, as shown in Figure 7.

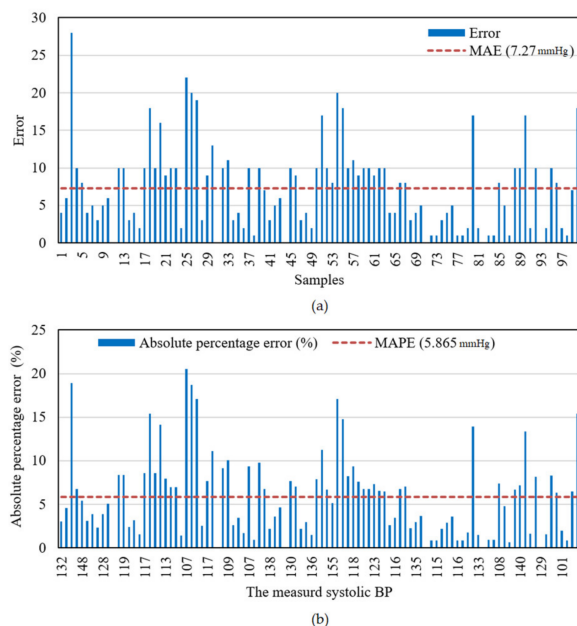


Figure 7. Error measurements of the systolic BP readings (a) an error with the number of samples (b) APE (%) relative to the systolic BM readings.

Figure 7a shows that the systolic BP error differs over the range from 0 mmHg to 27 mmHg with an MAE of 7.27 mmHg, whereas Figure 7b illustrates that the APE of the systolic BP readings differs over the 0–20.56% range of percentage with a MAPE of 5.865%. For the diastolic BP measurements, the error ratio is illustrated in Figure 8.

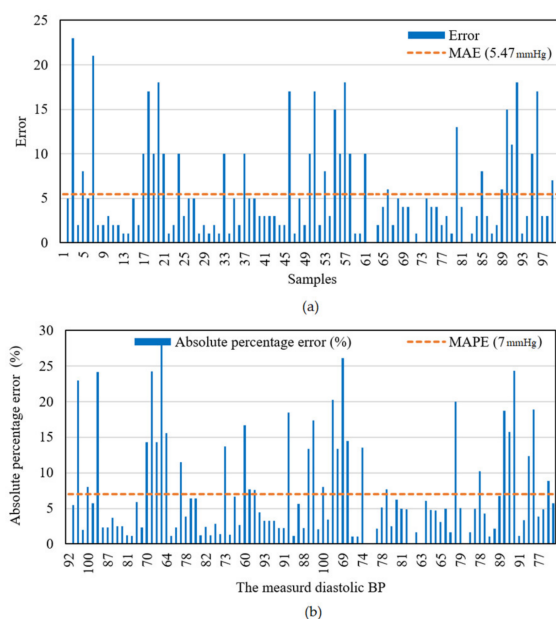


Figure 8. Error measurements of the diastolic BP readings (a) an error with the number of samples (b) APE (%) relative to the systolic BM readings.

Figure 8a shows that the diastolic error differs over the range from 0 mmHg to 23 mmHg with an MAE of 5.47 mmHg, and Figure 8b illustrates that the APE of the diastolic BP readings differs over the 0–28.125% range of percentage with a MAPE of 7%.

The proposed imaging system was also examined via statistical analysis, such as histogram test, probability density function (PDF), and cumulative density function (CDF). The measured BP readings by the proposed system firstly determined whether they were compatible with the benchmark measurements or not using a histogram test. The histogram test of the systolic BP data obtained from the proposed imaging system and the systolic BP data obtained from the benchmark is shown in Figure 9.

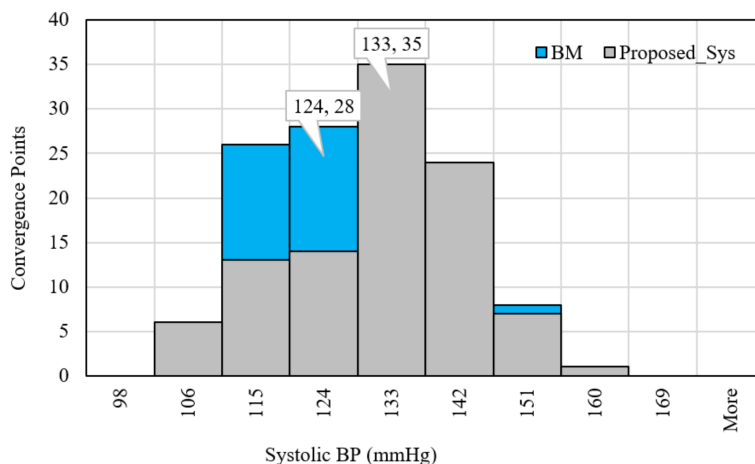


Figure 9. The histogram test of systolic BP data.

Figure 9 illustrates peaks of 35 and 28 points in the 133 and 124 mmHg classes for the proposed imaging system and the benchmark, respectively, leading to a good convergence between the proposed imaging system and the benchmark measurements. The histogram test of the diastolic BP data is shown in Figure 10.

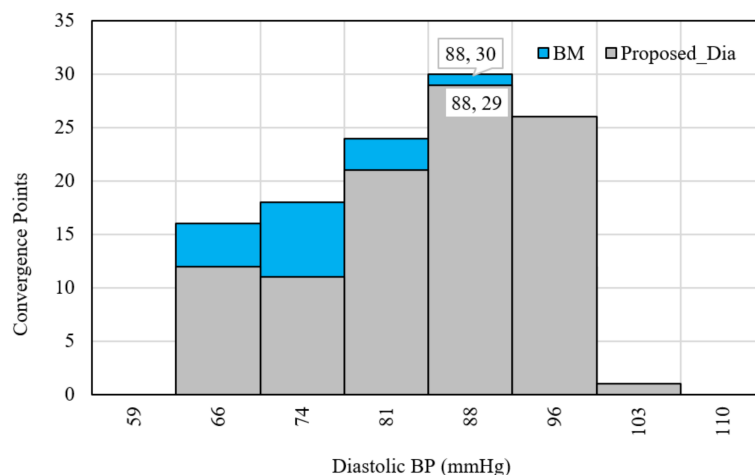


Figure 10. Histogram of the diastolic BP data.

Figure 10 reveals peaks of 29 and 30 points in the 88 and 88 mmHg classes for the proposed and the BM, respectively, leading to good convergence between the data measured by the proposed system and those measured by the benchmark. The measured BP data gained from the proposed imaging system were also investigated through a statistical metric based on a PDF test, as shown in Figures 11 and 12.

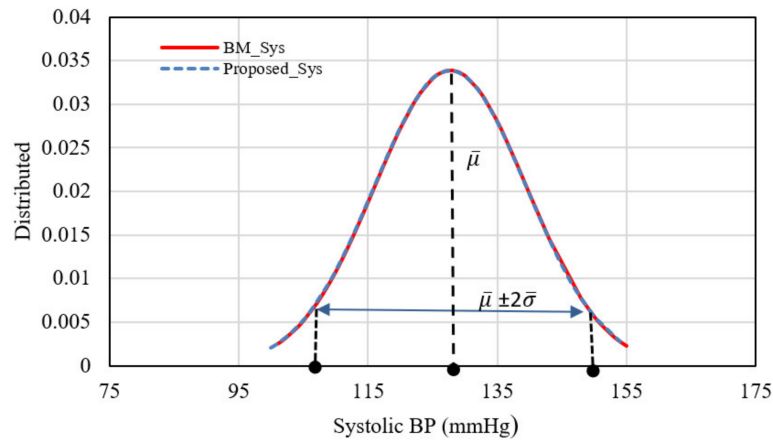


Figure 11. The PDF test of the systolic BP measurements against their corresponding benchmark measurements.

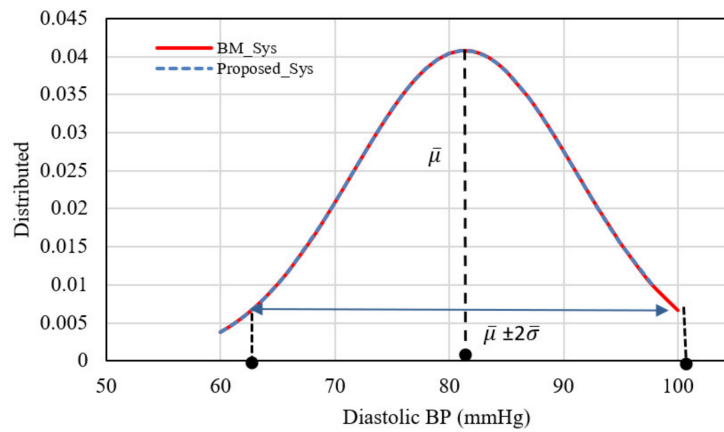


Figure 12. The PDF test of the diastolic BP measurements against their corresponding benchmark measurements.

Finally, the CDF plot was used for adjusting the distribution of BP measurements against their corresponding benchmark measurements, which preserves the relative relationship of the main data with a reference range. In this work, the CDF plot demonstrated a large agreement between systolic and diastolic BP measurements and the benchmark measurements, as shown in Figures 13 and 14, respectively.

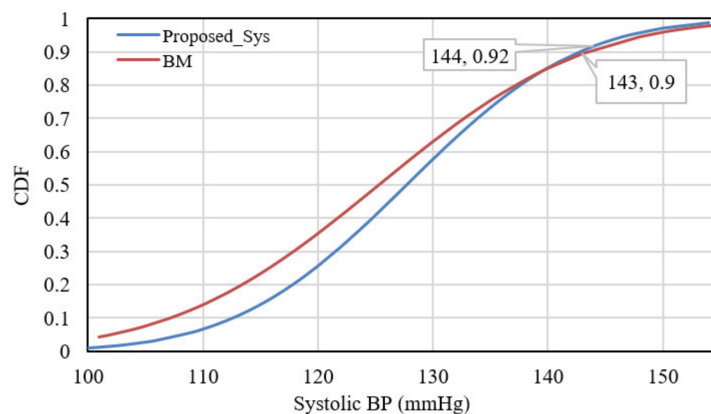


Figure 13. The CDF plot for systolic BP measurements.

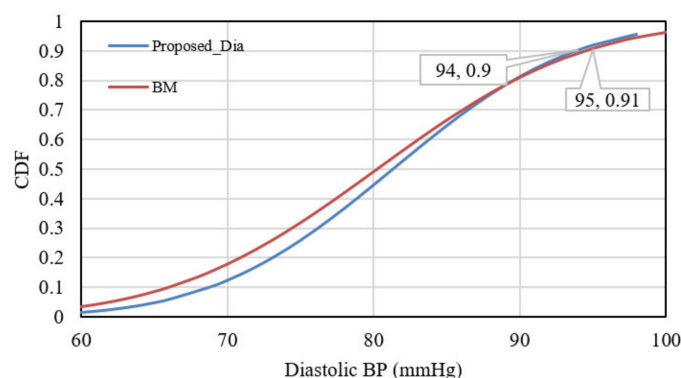


Figure 14. The CDF plot for diastolic BP measurements.

It is clear from Figure 13 that the CDF plot indicates a good agreement of 90% and 92% for systolic BP measurements values of 143 and 144 mmHg, respectively, whereas the CDF plot in Figure 14 indicates a better agreement of 94% and 95% for diastolic BP measurements values of 95 and 94 mmHg, respectively. The proposed imaging system achieves an average error percentage of 5.865% (Systolic BP) and 7% (Diastolic BP) compared to an average error percentage of 9.62% (Systolic BP) and 11.63% (Diastolic BP) obtained by [18], an average error percentage of 8.42% (Systolic BP) and 12.34% (Diastolic BP) obtained by [20], and an average error percentage of 9.28% (Systolic BP) and 9.84% (Diastolic BP) obtained by [21].

In addition to the lighting changes effects, the plethysmographic signals may be slightly affected by changing the subject's skin tone; therefore, this study recruited participants with different skin tones to increase the performance and accuracy of the proposed system. Through the data obtained, the error range of the obtained systolic BP falls within 7.27–9.2 mmHg, while it was 5.47–7.6 mmHg for the obtained diastolic BP compared to the benchmark measurements; this is because the benchmark measurements were also affected by movement artifacts and were inaccurate under some conditions, creating difficulty in the validation process with the proposed imaging system. Therefore, we tried to repeat the reference measurements until a steady reading was obtained. Additionally, the efficiency of the proposed imaging system is affected by subject movements, such as head rotation and facial expressions. It was also noticed that the proposed imaging system was inaccurate when perspiration was present on the forehead region or when it was covered with makeup, so all participants in the study were asked to clean and wipe the forehead region before filming. Finally, changing the distances between the camera and the face was not considered in this study.

4. Conclusions

In this study, a non-interventional imaging system was proposed to remotely estimate BP using plethysmographic video signals obtained from two regions of the forehead. The issue of illumination conditions that highly affected the plethysmographic signal was addressed using an efficient noise removal decomposition method. System performance was tested by comparing the error and the accuracy of the BP readings from the proposed imaging system, with the method showing promising results compared to the benchmark measurements. Thus, the proposed system makes the BP measurement potentially feasible and convenient for subjects, and also inexpensive, which is of great significance for healthcare applications and continuous vital signs monitoring.

Author Contributions: Conceptualization, A.A.-N.; Data curation, A.B.F. and M.F.M.; Formal analysis, A.A.-N. and M.F.M.; Funding acquisition, J.C.; Investigation, A.A.-N., A.B.F. and J.C.; Methodology, A.A.-N., A.B.F., M.F.M. and J.C.; Project administration, A.A.-N. and J.C.; Resources, M.F.M.; Software, A.A.-N.; Validation, A.A.-N. and A.B.F.; Writing—original draft, A.A.-N.; Writing—review & editing, A.B.F., M.F.M. and J.C. All authors have read and agreed to the published version of the manuscript.

Funding: This research received no external funding.

Data Availability Statement: Not applicable.

Conflicts of Interest: The authors declare no conflict of interest.

References

1. WHO. Cardiovascular Diseases (CVDs). Available online: [https://www.who.int/news-room/fact-sheets/detail/cardiovascular-diseases-\(cvds\)](https://www.who.int/news-room/fact-sheets/detail/cardiovascular-diseases-(cvds)) (accessed on 10 July 2022).
2. WHO. More Than 700 Million People with Untreated Hypertension. Available online: <https://www.who.int/news/item/25-08-2021-more-than-700-million-people-with-untreated-hypertension> (accessed on 13 July 2022).
3. Zhou, Y.; Ni, H.; Zhang, Q.; Wu, Q. The noninvasive blood pressure measurement based on facial images processing. *IEEE Sens. J.* **2019**, *19*, 10624–10634. [[CrossRef](#)]
4. Dawes, M.; Beerman, S.; Gelfer, M.; Hobson, B.; Khan, N.; Kuyper, L.; Mangat, B.; Tran, K.; Wilson, M.G.; Kaczorowski, J. The challenges of measuring blood pressure during COVID-19: How to integrate and support home blood pressure measurements. *Can. Fam. Physician* **2021**, *67*, 112–113. [[CrossRef](#)] [[PubMed](#)]
5. Xu, L.; Guo, X.; Yang, F.; Yin, S.; Zhang, X.; Meng, M.Q.-H. Implementation of cuff-less continuous blood pressure measurement system based on Android. In Proceedings of the 2012 IEEE International Conference on Information and Automation, Shenyang, China, 5–8 June 2012; pp. 552–556.
6. Junior, A.D.; Murali, S.; Rincon, F.; Atienza, D. Estimation of blood pressure and pulse transit time using your smartphone. In Proceedings of the 2015 Euromicro Conference on Digital System Design, Madeira, Portugal, 26–28 August 2015; pp. 173–180.
7. Li, H.; Zhao, H. Systolic blood pressure estimation using Android smart phones. In Proceedings of the 2013 6th International Conference on Biomedical Engineering and Informatics, Hangzhou, China, 16–18 December 2013; pp. 260–264.
8. Sagirova, Z.; Kuznetsova, N.; Gogiberidze, N.; Gognieva, D.; Suvorov, A.; Chomakhidze, P.; Omboni, S.; Saner, H.; Kopylov, P. Cuffless blood pressure measurement using a smartphone-case based ECG monitor with photoplethysmography in hypertensive patients. *Sensors* **2021**, *21*, 3525. [[CrossRef](#)] [[PubMed](#)]
9. Dinh, A.; Luu, L.; Cao, T. Blood pressure measurement using finger ECG and photoplethysmogram for IoT. In Proceedings of the International Conference on the Development of Biomedical Engineering in Vietnam, Ho Chi Minh, Vietnam, 27–29 June 2017; pp. 83–89.
10. Wang, E.J.; Zhu, J.; Jain, M.; Lee, T.-J.; Saba, E.; Nachman, L.; Patel, S.N. Seismo: Blood pressure monitoring using built-in smartphone accelerometer and camera. In Proceedings of the 2018 CHI Conference on Human Factors in Computing Systems, Montreal, QC, Canada, 21–26 April 2018; pp. 1–9.
11. Djeldjli, D.; Bousefsaf, F.; Maaoui, C.; Bereksi-Reguig, F.; Pruski, A. Remote estimation of pulse wave features related to arterial stiffness and blood pressure using a camera. *Biomed. Signal Process. Control* **2021**, *64*, 102242. [[CrossRef](#)]
12. Gambi, E.; Ricciuti, M.; Spinsante, S. Sensitivity of the contactless videoplethysmography-based heart rate detection to different measurement conditions. In Proceedings of the 2018 26th European Signal Processing Conference (EUSIPCO), Rome, Italy, 3–7 September 2018; pp. 767–771.
13. Al-Naji, A.; Khalid, G.A.; Mahdi, J.F.; Chahl, J. Non-contact SpO₂ prediction system based on a digital camera. *Appl. Sci.* **2021**, *11*, 4255. [[CrossRef](#)]
14. Al-Naji, A.; Gibson, K.; Lee, S.-H.; Chahl, J. Monitoring of cardiorespiratory signal: Principles of remote measurements and review of methods. *IEEE Access* **2017**, *5*, 15776–15790. [[CrossRef](#)]
15. McDuff, D.; Gontarek, S.; Picard, R.W. Remote detection of photoplethysmographic systolic and diastolic peaks using a digital camera. *IEEE Trans. Biomed. Eng.* **2014**, *61*, 2948–2954. [[CrossRef](#)] [[PubMed](#)]
16. Murakami, K.; Yoshioka, M.; Ozawa, J. Non-contact pulse transit time measurement using imaging camera, and its relation to blood pressure. In Proceedings of the 2015 14th IAPR International Conference on Machine Vision Applications (MVA), Tokyo, Japan, 18–22 May 2015; pp. 414–417.
17. Secerbegovic, A.; Bergsland, J.; Halvorsen, P.S.; Suljanovic, N.; Mujcic, A.; Balasingham, I. Blood pressure estimation using video plethysmography. In Proceedings of the 2016 IEEE 13th International Symposium on Biomedical Imaging (ISBI), Prague, Czech Republic, 3–16 April 2016; pp. 461–464.
18. Patil, O.R.; Gao, Y.; Li, B.; Jin, Z. CamBP: A camera-based, non-contact blood pressure monitor. In Proceedings of the 2017 ACM International Joint Conference on Pervasive and Ubiquitous Computing and Proceedings of the 2017 ACM International Symposium on Wearable Computers, Maui, HI, USA, 11–15 September 2017; pp. 524–529.
19. Sugita, N.; Yoshizawa, M.; Abe, M.; Tanaka, A.; Homma, N.; Yambe, T. Contactless technique for measuring blood-pressure variability from one region in video plethysmography. *J. Med. Biol. Eng.* **2019**, *39*, 76–85. [[CrossRef](#)]
20. Fan, X.; Ye, Q.; Yang, X.; Choudhury, S.D. Robust blood pressure estimation using an RGB camera. *J. Ambient Intell. Humaniz. Comput.* **2020**, *11*, 4329–4336. [[CrossRef](#)]
21. Zou, J.; Zhou, S.; Ge, B.; Yang, X. Non-Contact Blood Pressure Measurement Based on IPPG. *J. New Media* **2021**, *3*, 41. [[CrossRef](#)]
22. Iuchi, K.; Miyazaki, R.; Cardoso, G.C.; Ogawa-Ochiai, K.; Tsumura, N. Remote Estimation of Continuous Blood Pressure by a Convolutional Neural Network Trained on Spatial Patterns of Facial Pulse Waves. In Proceedings of the IEEE/CVF Conference on Computer Vision and Pattern Recognition, New Orleans, LA, USA, 19–20 June 2022; pp. 2139–2145.

23. Cheng, J.; Chen, X.; Xu, L.; Wang, Z.J. Illumination variation-resistant video-based heart rate measurement using joint blind source separation and ensemble empirical mode decomposition. *IEEE J. Biomed. Health Inform.* **2017**, *21*, 1422–1433. [[CrossRef](#)] [[PubMed](#)]
24. Viola, P.; Jones, M. Rapid object detection using a boosted cascade of simple features. In Proceedings of the 2001 IEEE Computer Society Conference on Computer Vision and Pattern Recognition, CVPR 2001, Kauai, HI, USA, 8–14 December 2001; pp. 511–518.
25. Lahiani, H.; Kherallah, M.; Neji, M. Hand pose estimation system based on Viola-Jones algorithm for android devices. In Proceedings of the 2016 IEEE/ACS 13th International Conference of Computer Systems and Applications (AICCSA), Agadir, Morocco, 29 November–2 December 2016; pp. 1–6.
26. Rabiha, S.G.; Kurniawan, A.; Moniaga, J.; Wilson, E.; Wahyudi, D.I. Face Authentication in E-Learning using Local Binary Pattern and Haar Cascade. In Proceedings of the 2018 International Seminar on Research of Information Technology and Intelligent Systems (ISRITI), Yogyakarta, Indonesia, 21–22 November 2018; pp. 28–32.
27. Khanam, F.-T.-Z.; Perera, A.G.; Alnaji, A.; Gibson, K.; Chahl, J. Non-contact automatic vital signs monitoring of infants in a neonatal intensive care unit based on neural networks. *J. Imaging* **2021**, *7*, 122. [[CrossRef](#)] [[PubMed](#)]
28. Poh, M.-Z.; McDuff, D.J.; Picard, R.W. Advancements in noncontact, multiparameter physiological measurements using a webcam. *IEEE Trans. Biomed. Eng.* **2010**, *58*, 7–11. [[CrossRef](#)] [[PubMed](#)]
29. Poh, M.-Z.; McDuff, D.J.; Picard, R.W. Non-contact, automated cardiac pulse measurements using video imaging and blind source separation. *Opt. Express* **2010**, *18*, 10762–10774. [[CrossRef](#)] [[PubMed](#)]
30. Khanam, F.-T.-Z.; Al-Naji, A.; Perera, A.G.; Gibson, K.; Chahl, J. Non-contact automatic vital signs monitoring of neonates in NICU using video camera imaging. *Comput. Methods Biomech. Biomed. Eng. Imaging Vis.* **2022**, 1–8. [[CrossRef](#)]
31. Colominas, M.A.; Schlotthauer, G.; Torres, M.E. Improved complete ensemble EMD: A suitable tool for biomedical signal processing. *Biomed. Signal Process. Control* **2014**, *14*, 19–29. [[CrossRef](#)]
32. Chen, D.-Y.; Wang, J.-J.; Lin, K.-Y.; Chang, H.-H.; Wu, H.-K.; Chen, Y.-S.; Lee, S.-Y. Image Sensor-Based Heart Rate Evaluation from Face Reflectance Using Hilbert–Huang Transform. *IEEE Sens. J.* **2015**, *15*, 618–627. [[CrossRef](#)]
33. Al-Naji, A.; Perera, A.G.; Chahl, J. Remote monitoring of cardiorespiratory signals from a hovering unmanned aerial vehicle. *Biomed. Eng. Online* **2017**, *16*, 101. [[CrossRef](#)] [[PubMed](#)]
34. Huang, N.E.; Shen, Z.; Long, S.R.; Wu, M.C.; Shih, H.H.; Zheng, Q.; Yen, N.-C.; Tung, C.C.; Liu, H.H. The empirical mode decomposition and the Hilbert spectrum for nonlinear and non-stationary time series analysis. *Proc. R. Soc. Lond. Ser. A Math. Phys. Eng. Sci.* **1998**, *454*, 903–995. [[CrossRef](#)]
35. Wu, Z.; Huang, N.E. Ensemble empirical mode decomposition: A noise-assisted data analysis method. *Adv. Adapt. Data Anal.* **2009**, *1*, 1–41. [[CrossRef](#)]
36. Torres, M.E.; Colominas, M.A.; Schlotthauer, G.; Flandrin, P. A complete ensemble empirical mode decomposition with adaptive noise. In Proceedings of the 2011 IEEE International Conference on Acoustics, Speech and Signal Processing (ICASSP), Prague, Czech Republic, 22–27 May 2011; pp. 4144–4147.